

Session 6:

ISM DIAGNOSTICS:

Dust

ISM Diagnostics: Dust

Takashi Onaka

Department of Astronomy, Graduate School of Science, The University of Tokyo
7-3-1 Hongo, Bunkyo-ku, Tokyo 113-0033, Japan
email: onaka@astron.s.u-tokyo.ac.jp

Abstract. Infrared (IR) observations provide significant information on the lifecycle of dust grains in the interstellar medium (ISM), which is crucial for the understanding of the evolution of matter in the universe. The IR spectral energy distribution (SED) of the dust emission tells us the relative abundance of sub-micron grains, very small grains, and carriers of the unidentified infrared (UIR) emission bands, since they emit the far-IR, the mid-IR, and the UIR bands from the near- to mid-IR, respectively. On the other hand, the UIR emission bands themselves offer a useful means to probe the physical conditions from which the band emission arises because each band is assigned to a specific C-H or C-C vibration mode and because its relative intensity should reflect the properties of the band carriers and the physical conditions of the environment. Here the two diagnostic methods using IR observations are briefly described together with examples of the observational results. Implications for the dust lifecycle are also discussed.

Keywords. ISM: general — dust, extinction — infrared: ISM — infrared: general

1. Introduction

Dust grains play significant roles in the interstellar medium (ISM). They absorb stellar radiation and emit the absorbed energy in the infrared (IR), controlling the thermal balance in the ISM. They also serve as a reservoir for heavy elements and play a key role in ISM chemistry. Hence their properties and variations in the ISM are important for the understanding of the evolution of matter in the universe. Dust grains are formed in the

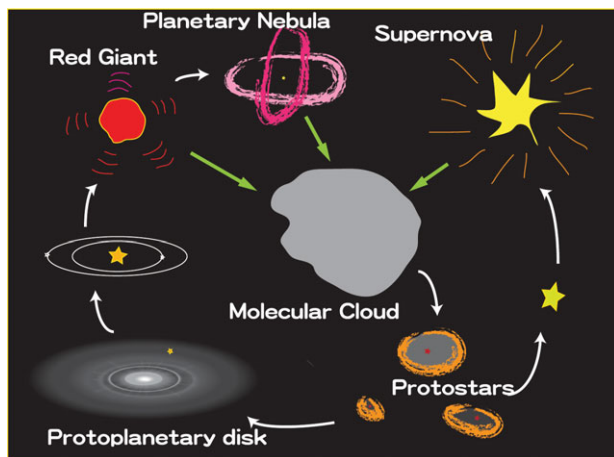


Figure 1. Dust lifecycle in the ISM. Heavy elements synthesized in the stellar interior are ejected to the ISM by mass-loss or explosions of evolved stars and a large fraction of them are condensed into dust grains. They are processed in the ISM and gathered to dense regions, being incorporated into newly-born stars.

outflow or ejecta of the material synthesized in the stellar interior, or in dense regions of the ISM, whereas they are processed and destroyed in the ISM (Fig. 1).

The dust lifecycle in the ISM has been becoming a popular topic in present-day astronomy (e.g., Jones 2004; Tielens 2005; Meixner *et al.* 2006). However, it has not yet been fully understood observationally where dust grains are formed and how they are processed and destroyed in the ISM. Recent space IR telescopes have been challenging this important issue and we are beginning to obtain a first picture of the dust lifecycle. In the following, two diagnoses of the dust properties in the ISM based on IR observations are described. Observational results using the diagnostic tools are also discussed.

2. Spectral Energy Distribution of the Dust Emission in the Infrared

IRAS observations found excess emission at $12\ \mu\text{m}$ in the diffuse Galactic radiation, which is far greater than the thermal emission expected from classical interstellar grains of sub-micron size that peaks at the far-infrared (FIR) (Boulanger *et al.* 1985). The excess emission is later shown to continue up to $60\text{--}80\ \mu\text{m}$ (Fig. 2), whereas the emission at $3\text{--}20\ \mu\text{m}$ is found to consist of a series of the emission bands, so-called the unidentified infrared (UIR) bands (Tanaka *et al.* 1996; Onaka *et al.* 1996). The UIR bands are thought to arise from polycyclic aromatic hydrocarbons (PAHs, Tielens 2008) or from amorphous organic solids with a mixed aromatic-aliphatic structure (Kwok & Zhang 2011). The excess emission is interpreted in terms of the stochastic heating of very small grains whose heat capacity is smaller than the typical energy of the incident radiation or the infrared fluorescence of PAHs. Dust models that have been constructed to account for the observed IR SED of the diffuse Galactic emission thus consist of sub-micron size big grains (BGs) that emit the FIR radiation, very small grains (VSGs) of nanometer size that give rise to the excess emission in $20\text{--}80\ \mu\text{m}$, and PAHs that carry the UIR band emission (e.g., Draine & Li 2001; Compiègne *et al.* 2011, see Fig. 2). The IR SED of the dust emission can tell us the relative abundance of BGs, VSGs, and PAHs, or a rough size distribution of interstellar dust grains once the intensity of the incident radiation field U is given, where U is defined in units of the solar neighborhood value. The change in the size distribution of dust grains can thus be investigated by IR SEDs.

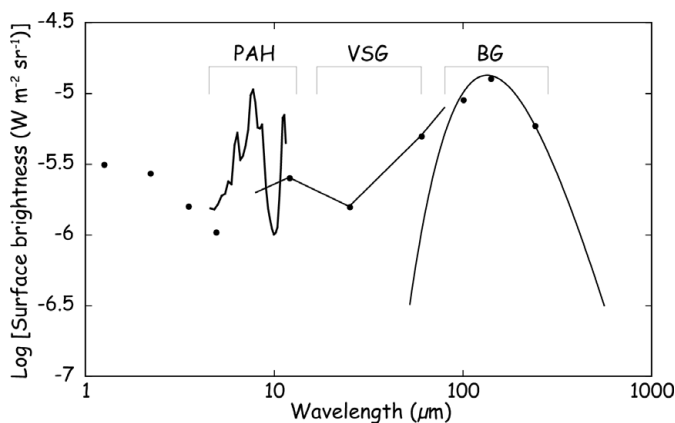


Figure 2. IR SED of the diffuse Galactic emission. The UIR band emission data in $5\text{--}12\ \mu\text{m}$ are taken from *IRTS* observations (Onaka *et al.* 1996) and other data points (black dots) are from *COBE/DIRBE* observations (Hauser *et al.* 1998). The spectral ranges where different dust components, BGs, VSGs, and PAHs, contribute are indicated by the thin lines (see text).

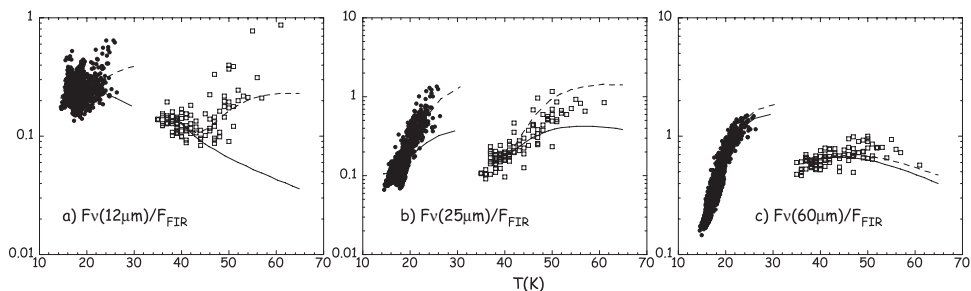


Figure 3. Ratios of the monochromatic intensities at 12, 25, and 60 μm to the total FIR intensity F_{FIR} for the Galactic plane (filled circles) and the Carina (open squares) region based on *IRTS* and *ISO* observations (Onaka *et al.* 2007b). The dashed lines indicate the SED model with the maximum radiation intensity $U_{\text{max}} = 10^5$ and the solid lines show those of $U_{\text{max}} = 10^4$. The Galactic plane and the Carina data are accounted for by the models with the minimum radiation intensity $U_{\text{min}} = 0.1$ and 5, respectively. In the model of the 12 μm emission, a decrease in the band emission at high U s is assumed. See Onaka *et al.* (2007b) for details of the calculation.

According to the stochastic heating model, the spectral shape of the excess emission as well as the band emission does not change with U , and the monochromatic intensity and the UIR band intensities are simply proportional to the total integrated FIR intensity F_{FIR} or the product of the incident radiation intensity U and the column density if the heating source is the same for BGs, VSG, and the band carriers (Onaka 2000). Figure 3 plots the monochromatic intensity at 12, 25, and 60 μm relative to F_{FIR} in the diffuse radiation from the Galactic plane and the Carina region against the temperature of BGs estimated from the FIR color. The data are taken from observations with *IRTS* and *ISO*. The 12 μm intensity decreases as the temperature becomes higher, which suggests destruction of the UIR band carriers in high U environments. The behaviors of the emission at 25 and 60 μm cannot be accounted for by a single U model, suggesting that there are components with different U s' on the line-of-sight. According to Dale *et al.* (2001), the distribution of U is introduced as a power-law function ($f(U) \propto U^{-\alpha}$ for $U_{\text{min}} < U < U_{\text{max}}$) and then the observations of the Galactic plane and the Carina region can be accounted for by the difference in the power-law index α and the minimum intensity of the incident radiation U_{min} on the line-of-sight (Onaka *et al.* 2007b). The distribution of U has to be taken into account in the diagnosis of the observed SED.

Draine *et al.* (2007) introduce a δ function of U_{min} to account for the general ISM contribution in addition to the power-law component, which represents the contribution from star-forming regions. They successfully fit IR SEDs of 65 SINGS galaxies observed with *Spitzer* (Kennicutt *et al.* 2003) by their dust models. One of the model parameters is the mass fraction of PAHs, q_{PAH} , which is derived for each galaxy. This model fit is made for the entire galaxy. If we have a spatially resolved dataset, the same analysis can derive the spatial distribution of q_{PAH} in a galaxy. Sandstrom *et al.* (2010) apply this method to *Spitzer* observations of the Small Magellanic Cloud (SMC) and find that the distribution of q_{PAH} shows a correlation with the CO map, but not with the stellar distribution, suggesting that the UIR band carriers are formed largely in dense regions in the SMC. On the other hand, Paradis *et al.* (2009) indicate that the distribution of q_{PAH} shows a correlation both with the CO intensity and the stellar distribution in the Large Magellanic Cloud (LMC) based on the *Spitzer* SAGE survey (Meixner *et al.* 2006), suggesting that the band carriers are supplied both from evolved stars and molecular clouds. Although further investigations are certainly needed for the understanding of the formation site of the UIR band carriers, these analyses clearly demonstrate the power of

the IR SED diagnostics for the investigation of the size distribution of dust grains and their formation process.

3. UIR Emission Bands

As described above, the mid-IR (MIR) excess emission in the diffuse Galactic radiation consists of a number of the emission bands (UIR bands). They are ubiquitously observed even in external galaxies (e.g., Smith *et al.* 2007). Each of the emission bands is assigned to a C-C or C-H bond vibration (e.g., Tielens 2008). Hence, their relative intensities can be used to probe the properties of the band carriers, such as the size distribution and the ionization degree, and/or the physical conditions from which these band emissions arise. For instance, the $3.3\ \mu\text{m}$ band is ascribed to an aromatic C-H stretching mode, while the $11.3\ \mu\text{m}$ band is attributed to a C-H out-of-plane vibration mode. Since both bands are unaffected by the ionization, the ratio of the $3.3\ \mu\text{m}$ to $11.3\ \mu\text{m}$ bands can be used as a good indicator of the band carrier size (the ratio becomes larger as the size becomes smaller) or the excitation of the carriers. Theoretical and laboratory studies indicate that the bands at 6.2 , 7.7 , and $8.6\ \mu\text{m}$ are enhanced by ionization. Therefore, for instance, the ratio of the $6.2\ \mu\text{m}$ to $11.3\ \mu\text{m}$ bands is an indicator of the ionization fraction of the band carriers. Recently the $8.6\ \mu\text{m}$ band is shown to be attributable to large, compact PAHs by theoretical investigations (Bauschlicher *et al.* 2008, 2009). This band may also be used as an indicator of the band carrier size. Since the UIR bands arise from the smallest members of dust grains, they are thought to be most sensitive to the change in the environmental conditions. The UIR bands offer a useful means to study the physical conditions and dust processing in the ISM.

Mori *et al.* (2012) analyze the spectra towards several positions in the LMC taken with the Infrared Camera (IRC) onboard *AKARI* (Onaka *et al.* 2007a). The IRC spectroscopy

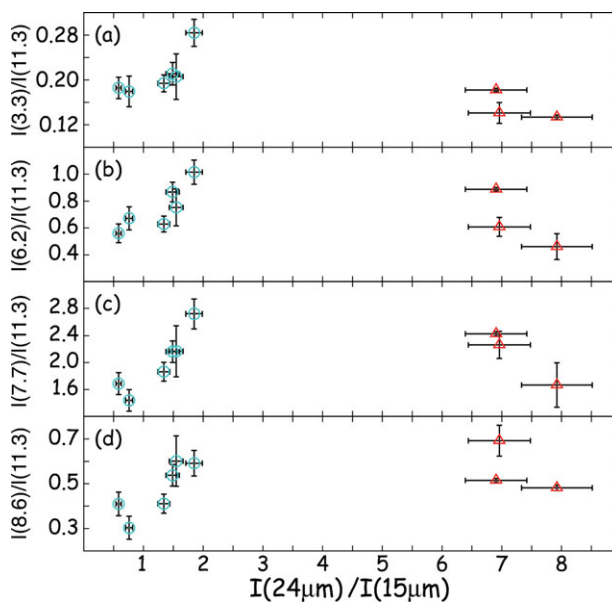


Figure 4. UIR band ratios vs. the infrared color of 24 to $11\ \mu\text{m}$ for the LMC targets based on observations with the IRC onboard *AKARI* (Mori *et al.* 2012). (a) $3.3\ \mu\text{m}$ band, (b) $6.2\ \mu\text{m}$ band, (c) $7.73\ \mu\text{m}$ band, and (d) $8.6\ \mu\text{m}$ band to the $11.3\ \mu\text{m}$ band intensities. The blue open circles indicated the PDR targets, while the red open triangles show the HII region targets.

has a unique characteristic that enables it to take a spectrum from 2.5 to 13 μm at the same slit simultaneously (Ohyama *et al.* 2007). Thus, the band emission in this spectral range can directly be compared with each other without correcting for the slit size. Figure 4 plots the various band ratios against the IR color of the 24 to 11 μm , which is also taken with the IRC (Ita *et al.* 2008). The 24 to 11 μm color is generally thought to indicate the star-formation activity since the thermal emission of high-temperature BGs contributes to an increase in the intensity at 24 μm according to the SED model (see Fig. 3). Figure 4 indicates that there are two classes of objects in the present targets. The spectra of the data located in the left (open circles) do not show ionized gas signatures, such as hydrogen recombination lines, and thus the emission towards those targets are dominated by photon-dominating regions (PDRs). On the other hands, those at the right (open triangles) show ionized gas signatures clearly and their emission is dominated by HII regions. The data of the PDRs show a clear trend that the band ratios increase with the IR color, thus with the star-formation activity, while the HII region data neither follow the trend nor show a systematic trend. The trend seen in the PDR targets indicates that the excitation degree (as indicated by the 3.3 to 11.3 μm band ratio) and the ionization fraction (as indicated by the other three band ratios) of the band carriers also increase with the IR color, suggesting that the incident radiation field becomes harder as its intensity increases. In the SED model described in the previous section, an increase of the 24 μm intensity can be accounted for by an increase of U , but it does not change the band ratios since the spectrum of the incident radiation is fixed and only the intensity U is changed. The IRC data suggest for the first time that the spectrum of the incident radiation also becomes harder as U increases in PDRs.

Figure 5 shows the two band-ratio diagram of the 3.3 to 11.3 μm and the 7.7 to 11.3 μm band ratios for the PDR targets (a) and the HII region targets (b). As described above, the 3.3 to 11.3 μm band ratio is an indicator of the size or excitation degree of the UIR band carriers, while the 7.7 to 11.3 μm band ratio suggests the ionization fraction. The data of the PDR targets show a clear sequence. To investigate the sequence quantitatively,

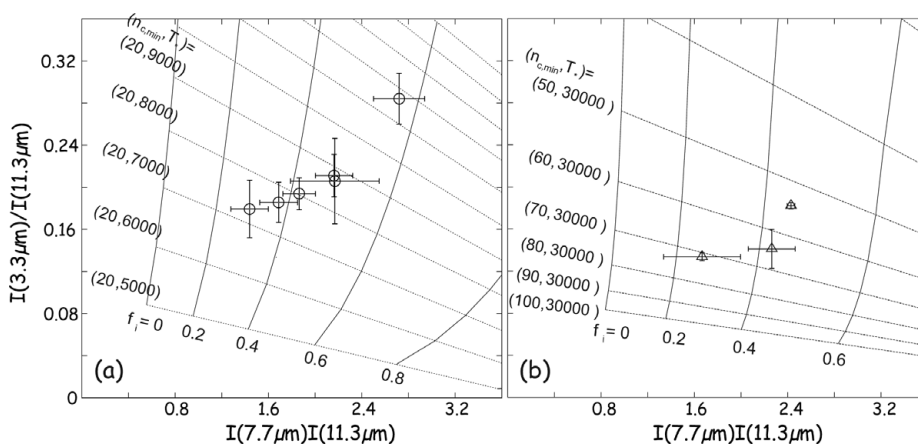


Figure 5. Two band-ratio diagram of the 3.3 to 11.3 μm vs. the 7.7 to 11.3 μm band ratios for the LMC targets (Mori *et al.* 2012). (a) PDR targets (open circles) and (b) HII region targets (open triangles). In (a), a model grid of the ionization fraction f_i and the effective temperature T_* of the exciting source is overplotted. The number of carbon atoms in the smallest UIR band carrier $n_{c,\text{min}}$ is fixed as 20. In (b), a model grid of the ionization fraction f_i and the the number of carbon atoms in the smallest band carrier $n_{c,\text{min}}$ is plotted. The effective temperature T_* of the exciting source is fixed at 30000 K.

a simple model grid is calculated and overplotted (see Mori *et al.* (2012) for details of the model calculation). The grid is constructed by changing the effective temperature of the exciting source T_* and the ionization fraction of the band carriers f_i . The number of carbon atoms in the smallest band carrier $n_{c,\min}$ is fixed at 20 in the grid of Fig. 4a, assuming that the size distribution does not change among the PDR targets. The observed trend can be interpreted fairly well in terms of the increase of the ionization fraction together with the increase of T_* as expected from the above discussion.

The data of the HII region targets cannot be accounted for by the same model grid (Fig. 5b). Their ratios of the 7.7 to 11.3 μm bands are in a range similar to those of the PDR targets, which can be interpreted by the fact that the enhanced photoionization in HII regions is compensated by the increase in the recombination due to the increase of the electron density and thus the ionization fraction does not change appreciably even in HII regions. However, the 3.3 to 11.3 μm band ratio of the HII region targets cannot be accounted for since HII regions should have a higher T_* and thus higher band ratios are expected. To investigate a possible interpretation, a new model grid is constructed by changing $n_{c,\min}$ instead of T_* , which is fixed as 30000 K, as shown in Fig. 5b. The new model grid suggests that the observations of the HII region targets can be explained by the paucity of small band carriers. Although previous studies indicate a decrease of the UIR band emission in ionized regions or under intense radiation environments (e.g., Dale *et al.* 2001; Onaka 2004; Povich *et al.* 2007), the IRC observations clearly show that the decrease proceeds from small band carriers. This is in agreement with the prediction of the sputtering process in HII regions (Micelotta *et al.* 2010).

Although the UIR band intensity ratios are a useful tool, only small variations in the band ratios have so far been reported for the diffuse Galactic radiation (e.g., Chan *et al.* 2001; Sakon *et al.* 2004). Even in the data of the LMC shown in Fig. 5, the variations are typically 20–30% and less than a factor of 2. The most extreme cases are seen in elliptical galaxies or galaxies with low-luminosity AGNs. Kaneda *et al.* (2005) report that in elliptical galaxies, the 11.3 μm band emission is clearly seen, but the 6.2 and 7.7 μm bands are very weak or absent, while Smith *et al.* (2007) indicate that galaxies with low-luminosity AGNs tend to show weaker 7.7 μm band emission relative to the 11.3 μm band (Fig. 6). The *AKARI* spectrum of the elliptical galaxy NGC1316 (Fornax A) shows only the 11.3 μm band emission and no 3.3, 6.2, 7.7, and 8.6 μm band emission (Kaneda *et al.* 2007), which suggests the dominance of large, neutral band carriers in this galaxy. The absence of the 3.3 μm band crucially suggests the absence of small band carriers. The AGN of this galaxy ceased 100 Myr ago, which is much longer than the typical lifetime of the UIR band carriers, suggesting that the AGN may not be a key factor for the unusual UIR band strengths.

Low-metallicity dwarf galaxies offer an interesting place to investigate the formation and destruction processes of the UIR band carriers. Several investigations suggest that the UIR band emission disappears below $12 + \log(O/H) \sim 8.1$ (e.g., Smith *et al.* 2007; Engelbracht *et al.* 2008; Wu *et al.* 2011). Recently Hunt *et al.* (2010) show that the presence or absence of the UIR band emission is not a unique function of the metallicity, but it is rather controlled by the hardness of the radiation field based on observations of 22 blue compact dwarf (BCD) galaxies with the IRS onboard *Spitzer*. They further suggest that BCDs tend to show the stronger 8.6 and 11.3 μm band emissions relative to the 6.2 and 7.7 μm band emissions than the average of starburst galaxies. If the 8.6 μm band emission comes predominantly from large band carriers, it is suggested that only large band carriers survive in intense radiation field environments as in BCDs.

Sandstrom *et al.* (2012) analyze spectroscopic data of the selected regions in the SMC taken with the *Spitzer*/IRS. They found that compared to the average of the SINGS

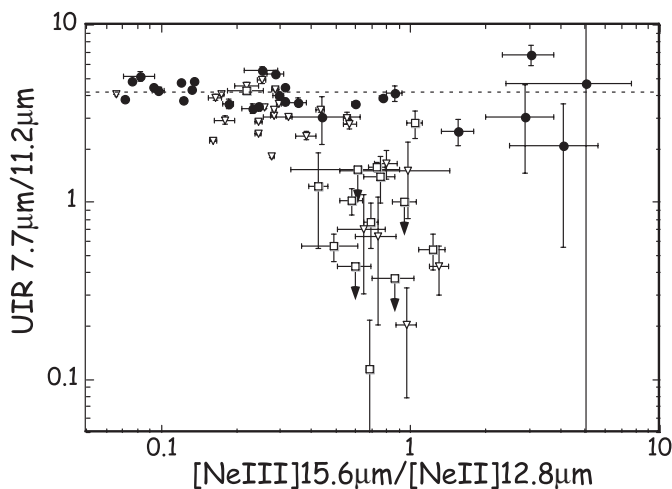


Figure 6. Intensity ratio of the 7.7 to 11.3 μm bands against the ratio of the [NeIII]15.6 μm to [NeII]12.8 μm line intensities. The SINGS galaxy data are taken from Smith *et al.* (2007). Galaxies with HII-dominated nuclei are indicated by the filled circles and those with low-luminosity AGNs by the open triangles. Elliptical galaxy data taken from Kaneda *et al.* (2008) are shown by the open squares. The dotted line indicates the median of the HII-dominated galaxies. Those located at the large [NeIII]/[NeII] region are blue compact dwarfs.

galaxies, the SMC data show the relatively weak 8.6 μm and strong 11.3 μm band emissions, suggesting that the UIR band carriers in the SMC are smaller and less ionized than in the SINGS galaxies. The dominance of smaller band carriers cannot be explained by the sputtering process and may reflect the formation process at the low metallicity conditions of the SMC. It is suggested that in low-metallicity galaxies, small band carriers are preferentially formed and thus easily susceptible to destruction in the ISM.

One of the key measures for the size distribution of the UIR band carriers is the 3.3 μm band emission as indicated in the LMC data. The *Spitzer* IRS spectrum of the disk of the nearby BCD NGC1569, whose metallicity is $12 + \log(O/H) \sim 8.13$, being at the threshold of the UIR band presence, clearly shows the UIR bands emission. *AKARI* spectroscopy indicates that the 3.3 μm varies significantly over small spatial scales in the disk, but the ratio of the 3.3 to 11.3 μm band intensities in the disk is at most 0.2. Compared to Fig. 5, it is still smaller than the average of the PDRs, suggesting a paucity of small band carriers in the disk of NGC1569. The UIR band emission is also detected in one of the H α filaments in NGC1569 (Onaka *et al.* 2010). The marginal detection of the 3.3 μm band as well as the weak 8.6 μm band emission in the filament suggests that small UIR band carriers may be formed in the shock at the filament.

4. Summary

IR observations provide significant information on the study of the properties and processing of dust grains in the ISM. Observations with the latest space infrared telescopes are now beginning to show us a first view of the dust lifecycle in the ISM. IR SEDs can tell us the relative abundance of BGs, VSGs, and PAHs, and thus variations in the size distribution of dust in various environments. The UIR band emission is very useful to probe the physical conditions and properties of the band carriers. They can tell us details of the destruction processes in various environments. The 3.3 μm band emission gives crucial information on the abundance of small band carriers.

Acknowledgements

This work was based on observations with *IRTS*, *ISO*, *Spitzer* and *AKARI*. *IRTS* is a joint mission between ISAS and NASA, managed and operated by ISAS. *ISO* is an ESA project with instruments funded by ESA Member States (especially the PI countries: France, Germany, the Netherlands and the United Kingdom) and with the participation of ISAS and NASA. *Spitzer* is operated by Jet Propulsion Laboratory, California Institute of Technology, under NASA contract 1407 and *AKARI* is a JAXA project with the participation of ESA. The author thanks D. Tokura, H. Matsumoto, Y. Okada, I. Sakon, R. Ohsawa, T. I. Mori, and H. Kaneda for their contributions. This work is supported by a Grant-in-Aid for Scientific Research the Japan Society for the Promotion of Science.

References

- Bauschlicher, C. W., Jr., Peeters, E., & Allamandola, L. J. 2008, *ApJ*, 678, 316
 Bauschlicher, C. W., Jr., Peeters, E., & Allamandola, L. J. 2009, *ApJ*, 697, 311
 Boulanger, F., Baud, B., & van Albada, G. D. 1985, *A&A*, 144, L9
 Chan, K.-W., Roellig, T. L., Onaka, T., *et al.* 2001, *ApJ*, 546, 273
 Compiègne, M., Verstraete, L., Jones, A., *et al.* 2011, *A&A*, 525, 103
 Dale, D. A., Helou, G., Contursi, A., Silbermann, N. A., & Kolhatkar, S. 2001, *ApJ*, 549, 1886
 Draine, B. T., & Li, A. 2001 *ApJ*, 551, 807
 Draine, B. T., Dale, D. A., Bendo, G., *et al.* 2007, *ApJ*, 663, 866
 Engelbracht, C. W., Rieke, G. H., Gordon, K. D., *et al.* 2008, *ApJ*, 678, 804
 Hauser, M. G., Arendt, R. G., Kelsall, T., *et al.* 1998, *ApJ*, 508, 25
 Hunt, L., Thuan, T. X., Izotov, Y. I., & Sauvage, M. 2010, *AJ*, 712, 164
 Ita, Y., Onaka, T., Kato, D., *et al.* 2008, *PASJ*, 60, S435
 Jones, A. P. 2004, *ASP conf. ser.* 309, 347
 Kaneda, H., Onaka, T., & Sakon, I. 2005, *ApJ*, 632, L83
 Kaneda, H., Onaka, T., & Sakon, I. 2007, *ApJ*, 666, L21
 Kaneda, H., Onaka, T., Sakon, I., Kitayama, T., Okada, T., & Suzuki, T. 2008, *ApJ*, 684, 270
 Kennicutt, R. C., Jr., Armus, L., Bendo, G., *et al.* 2003, *PASP*, 115, 928
 Kwok, S. & Zhang, Y. 2011, *Nature*, 479, 80
 Meixner, M., Gordon, K. D., Indebetouw, R., *et al.* 2006, *AJ*, 132, 2288
 Micelotta, E. R., Jones, A. P., & Tielens, A. G. G. M. 2010, *A&A*, 510, 37
 Mori, T. I., Sakon, I., Onaka, T., Kaneda, H., Umehata, H., & Ohsawa, R. 2012, *ApJ*, 744, 68
 Ohya, Y., Onaka, T., Matsuhara, H., *et al.* 2007, *PASJ*, 59, S411
 Onaka, T., Yamamura, I., Tanabeé, Roellig, T. L., & Yuen, L. 1996, *PASJ*, 48, L59
 Onaka, T. 2000, *Adv. Sp. Res.*, 25, 2167
 Onaka, T. 2004, *ASP conf. ser.* 309, 163
 Onaka, T., Matsuhara, H., Wada, T., *et al.* 2007a, *PASJ*, 59, S401
 Onaka, T., Tokura, D., Sakon, I., Tajiri, Y. Y., Takagi, T., & Shibai, H. 2007b, *ApJ*, 654, 844
 Onaka, T., Matsumoto, H., Sakon, I., & Kaneda, H. 2008, *IAU Symp.* 251, 229
 Onaka, T., Matsumoto, H., Sakon, I., & Kaneda, H. 2010, *A&A*, 514, A15
 Paradis, D., Reach, W., Berdard, J.-P., *et al.* 2009, *ApJ*, 138, 196
 Povich, M., Stone, J. M., Churchwell, E., *et al.* 2007, *ApJ*, 660, 346
 Sakon, I., Onaka, T., Ishihara, D., *et al.* 2004, *ApJ*, 609, 203 (Erratum: *ApJ*, 625, 1062)
 Sandstrom, K. M., Bolatto, A., Draine, B. T., Bot, C., & Stanimirović, S. 2010, *ApJ*, 715, 701
 Sandstrom, K. M., Bolatto, A., Bot, C., *et al.* 2012, *ApJ*, 744, 20
 Smith, J. D. T., Draine, B. T., Dale, D. A., *et al.* 2007, *ApJ*, 656, 770
 Tanaka, M., Matsumoto, T., Murakami, H., *et al.* 1996, *PASJ*, 48, L53
 Tielens, A. G. G. M., 2005, *The Physics and Chemistry of the Interstellar Medium* (Cambridge, UK: Cambridge University Press)
 Tielens, A. G. G. M., 2008, *ARAA*, 46, 289
 Wu, R., Hogg, D. W., & Moustakas, J. 2011, *ApJ*, 730, 111